Author Manuscript

Author Manuscript

Author Manuscript

Author Manuscript

HHS Public Access

Author manuscript

Nat Chem. Author manuscript; available in PMC 2021 February 28.

Published in final edited form as:

Nat Chem. 2020 October ; 12(10): 906–913. doi:10.1038/s41557-020-0530-4.

Using Sulfuramidimidoyl Fluorides that Undergo Sulfur(VI) Fluoride Exchange for Inverse Drug Discovery

Gabriel J. Brighty[1,2,†], **Rachel C. Botham**[1,2,†], **Suhua Li**[1,†], **Luke Nelson**[1], **David E. Mortenson**[1,2], **Gencheng Li**[1], **Christophe Morisseau**[3,4], **Hua Wang**[1], **Bruce D. Hammock**[3,4], **K. Barry Sharpless**[1,5], **Jeffery W. Kelly**[1,2,5]

[1]Department of Chemistry, The Scripps Research Institute, La Jolla, CA 92037

[2]Department of Molecular Medicine, The Scripps Research Institute, La Jolla, CA 92037

[3]Department of Entomology and Nematology, University of California Davis, Davis, CA 95616

[4]UC Davis Comprehensive Cancer Center, University of California Davis, Davis, CA 95616

[5]The Skaggs Institute for Chemical Biology, The Scripps Research Institute, La Jolla, CA 92037

Abstract

Drug candidates that form covalent linkages with their target proteins have been under-explored compared to conventional counterparts that modulate biological function by reversible binding to proteins, in part due to concerns about off-target reactivity. But toxicity linked to off-target reactivity can be minimized by using latent electrophiles that only become activated towards covalent bond formation upon binding a specific protein. Here, we study sulfuramidimidoyl fluorides (SAFs), a class of weak electrophiles that undergo sulfur(VI) fluoride exchange (SuFEx) chemistry. We show that equilibrium binding of a SAF to a protein can allow nucleophilic attack by a specific amino acid side chain leading to conjugate formation. Sixteen small molecules, each bearing a SAF electrophile, were incubated with human cell lysate, and the protein conjugates formed were identified by affinity chromatography–mass spectrometry. This inverse drug discovery approach identified a compound that covalently binds to, and irreversibly inhibits the activity of PARP1, an important anti-cancer target in living cells.

Users may view, print, copy, and download text and data-mine the content in such documents, for the purposes of academic research, subject always to the full Conditions of use:http://www.nature.com/authors/editorial_policies/license.html#termsReprints and permissions information is available at www.nature.com/reprints

Correspondence and requests for materials should be addressed to J.W.K. at jkelly@scripps.edu or K.B.S. at sharples@scripps.edu.

Author contributions

G.J.B., R.C.B., J.W.K. Conceived and designed the experiments

G.J.B., R.C.B., S.L., L.N., D.E.M., G.L., C.M., H.W. carried out experiments and performed data analysis

G.J.B., R.C.B., S.L., C.M., B.D.H., K.B.S., J.W.K. co-wrote the paper

†These authors contributed equally to this work

‡Present addresses: R.C.B. Codexis, Redwood City, CA 94063, S.L. School of Chemistry, Sun Yat-Sen University, Guangzhou, P.R.China, D.E.M. Gilead Sciences Inc., Foster city, CA 94404, H.W. Sorrento Therapeutics, Inc., San Diego, CA 92121

Supplementary Information

Supplementary information is linked to the online version of the paper at www.nature.com/nature

Competing Interests

The authors declare no competing interests.

Author Manuscript Author Manuscript Author Manuscript Author Manuscript

In conventional drug discovery approaches, a large number of small molecules are screened for their ability to modify the function of an isolated target protein or a particular cellular phenotype[1]. These approaches can yield hits that exert their action by both covalent and non-covalent mechanisms. Drugs that form covalent conjugates with their targets have historically been avoided due to off-target toxicity concerns, but they can offer potential benefits over non-covalent inhibitors in terms of increased duration of action, lower dosing, and the possibility of decreased development of resistance[2,3]. Therefore, we have developed the Inverse Drug Discovery (IDD) strategy, which involves individually reacting a small collection of diverse organic compounds harbouring a weak, but activatable electrophile with the human proteome in cell lysate to identify the protein(s) targeted[4]. This method identifies numerous nucleophilic sites within the human proteome using only a handful of mildly reactive compounds.

An earlier IDD study using arylfluorosulfates, activated toward covalent bond formation by the geometry and composition of the complementary protein binding sites, afforded both enzyme and non-enzyme conjugates[4]. From this study, we learned that the presence of a suitable protein binding pocket allows the electrophilic sulfur center to be placed proximal to a tyrosine or lysine side-chain nucleophile, enabling the Sulfur(VI) Fluoride Exchange (SuFEx) reaction to proceed[4–6]. The additional presence of a nearby cationic arginine and/or lysine side chain seem to be critical for lowering the barrier for the SuFEx reaction, as these residues likely facilitate extraction of the fluoride ion. These cationic residues may also perturb the reactive side-chain's pKa, enhancing its nucleophilicity[4]. The potential of SuFEx reactions employing sulfonyl fluorides and arylfluorosulfates has been demonstrated in the fields of material science[7–9] and late stage drug functionalization enhancing non-covalent activity[10].

Herein, we apply the IDD approach[4,6] to another family of SuFEx-derived electrophiles, the sulfuramidimidoyl fluorides (SAFs)[11], whose proteome reactivity has not been previously assessed. We explore the hypothesis that the unique chemical environments within proteins should allow the use of less reactive SuFEx-derived SAFs for IDD. SAFs are prepared by a two-step SuFEx reaction process[11]. First, an alkyl or aryl primary amine is reacted with thionyl tetrafluoride (SOF_4) at standard temperature and pressure, in the presence of two equivalents of an organic base to produce the corresponding iminosulfur oxydifluoride. Next, a secondary amine displaces one of the remaining fluorides in the presence of a single equivalent of organic base to produce the corresponding SAF (Fig. 1a). The reduced electrophilicity of SAFs compared to arylfluorosulfates in acetonitrile likely arises from the replacement of a S=O bond with a S=NR bond, increasing the electron density around the sulfur center in SAFs, affording an even stronger bond between the fluorine and sulfur[11]. Although the sulfur centers in both SAFs and arylfluorosulfates are tetrahedral, in SAFs this center is also chiral[11].

In this study, we matched SAFs with the human protein(s) that they react with using affinity chromatography–mass spectrometry. Select conjugation reactions were then validated using recombinant proteins *in vitro*. We demonstrate that structurally distinct SAFs react with different sets of human proteins. Lastly, we matched a thymidine-based SAF with Poly(ADP-Ribose) Polymerase 1 (PARP1), and demonstrated covalent inhibition of PARP1

Author Manuscript Author Manuscript Author Manuscript Author Manuscript

both *in vitro* and in live cells, potentially complementing the non-covalent PARP1 inhibitors used to ameliorate cancer.

Results

SAFs react with human proteins

We set out to survey the human proteome for its reactivity with 16 SAF-containing compounds (Fig. 1b). Compounds **1**–**16** comprised largely unpublished SAFs harbouring terminal acetylenes available at the outset of this study[11]. We purposefully did not try to select for motifs that would bind to a particular protein family, although we did use our intuition to maximize structural diversity. Each SAF was individually incubated with HEK293T cell lysate for 18 h. The extent of reaction between a given SAF and the targeted proteins increases linearly over 24 h (Supplementary Fig. 1). Therefore, we chose an 18 h incubation period as a practical experimental time point in order to capture sufficient quantities of SAF-conjugated proteins. The 16 conjugation reactions were then subjected to a copper(I)-catalyzed azide-alkyne cycloaddition (CuAAC) reaction[12,13] with tetramethylrhodamine azide (TMR-N_3) and the conjugates were separated in a denaturing gel (SDS-PAGE) visualized by tetramethylrhodamine fluorescence (Fig. 1c). Notably, compounds **1**–**16** display different reactivity profiles toward the human proteome detectable by SDS-PAGE, indicating that equilibrium binding fragments of these compounds are critical determinants of selectivity for the conjugation process. To more comprehensively survey the conjugates formed and to detect lower abundance conjugates, we utilized quantitative liquid chromatography-mass spectrometry (LC-MS/MS)[4].

Proteomics Identifies the Targets of SAFs 1–16

To identify the human proteins targeted by SAFs **1**–**16**, we subjected the sixteen proteome labeling reactions to CuAAC reactions with a reductively cleavable biotin azide (biotin-N_3)[12–14] after an 18 h incubation at 25 ˚C. The SAF-conjugated proteins were subsequently enriched *via* streptavidin affinity chromatography. Sodium dithionite ($Na_2S_2O_4$) was used to elute the bound proteins from the streptavidin resin. Enriched proteins were then digested with trypsin and subjected to tandem-mass tag (TMT) labeling[15] to enable quantification of the SAF-protein conjugates relative to a proteome cell lysate sample treated with DMSO (vehicle; otherwise identically treated) by LC-MS/MS (Fig. 2a). We defined the enrichment ratio for each protein as the average of the TMT reporter ion intensity for a given protein in the SAF-treated samples / average of TMT reporter ion intensity for that same protein in the vehicle-treated samples. Proteins were ranked according to this enrichment ratio. Duplicate measurements of each treatment condition (SAF treated vs. DMSO treated) were compared by their enrichment ratios and statistical significance to assess the reliability of each protein target identification. We prioritized protein “hits” that exhibited strong enrichment relative to vehicle treated (enrichment ratios > 1.5) and reasonable statistical agreement between duplicate measurements (p-values < 0.25). Additionally, we noted the strong enrichment of several proteins with different SAFs, further indicating that these proteins are reactive towards SAFs.

Author Manuscript Author Manuscript Author Manuscript Author Manuscript

As observed in the SDS-PAGE-based comparisons (Fig. 1c), LC-MS/MS analysis of SAFs **1**–**16** reacting with human cell lysate (HEK293T) revealed substantial differences in the set of protein conjugates formed from distinct SAFs (Fig. 2b; depicting a sampling of SAF-reactive proteins). The SAFs appear to target proteins with a variety of functions, including both enzymes and non-enzymes (Supplementary Fig. 2a & 2b). Structural proteins and proteins that bind RNA were just a couple of the molecular functions enriched for (enrichment over DMSO > 1.5 and p-value < 0.25) by SAFs **1**–**16**. Among the identified proteins were GSTP1, NME1, and CRABP2, all of which have previously demonstrated reactivity towards arylfluorosulfates[4,6]. Notably, we found strong enrichment of several therapeutically important proteins that were not previously targeted by arylfluorosulfates. These include PARP1 and PARP2, critical members of DNA damage repair pathways and validated therapeutic targets for BRCA-mutant-associated breast and ovarian cancers[16,17]. Also targeted were macrophage movement inhibitory factor (MIF), which enhances the metastatic potential of certain cancers and acts as a pro-inflammatory signal in both chronic and acute inflammatory diseases[18,19]; soluble epoxide hydrolase (EPHX2), which has garnered attention as a pharmacological target for the treatment of certain cardiovascular diseases[20]; and branched chain amino acid transaminase 1 (BCAT1), which is a therapeutic target for myeloid leukemia, carcinoma, glioblastoma, and certain breast cancers[21–23]. While we observed enrichment for 137 proteins that have been targeted by other SuFEx-derived electrophiles, more than 72% of the 491 proteins identified by SAFs **1**–**16** are distinct from those that have been identified using arylfluorosulfates[4,6] or sulfonyl fluorides[24–27] (Supplementary Fig. 2c).

Validation of Select SAF-Protein Reactions

In order to validate SAF-reactive proteins identified by affinity chromatography–MS/MS, we expressed and purified four therapeutically important proteins and reacted each purified protein with either a SAF exhibiting a high enrichment ratio (a “positive” hit) or one that afforded a low or no enrichment (a “negative” hit). For PARP1 we expressed only the catalytic domain (PARP1cat). Compounds **13**, **11**, **9**, and **2** were selected as the positive “hits” for MIF, BCAT1, EPHX2, and PARP1cat, respectively, while compounds **10**, **1**, **15**, and **11** were selected as negative “hits” for the same proteins, respectively. After an 18 h reaction period, each protein (3 μM) was subjected to CuAAC reactions with TMR-N_3 and the conjugates were separated by SDS-PAGE and visualized by fluorescence (Fig. 3a). In all four cases, the “positive” hits reacted more than the “negative” hits with their respective proteins, exhibiting statistical significance (Fig. 3b). It appeared that neither BCAT1 nor EPHX2 were particularly reactive towards their SAF probes. This may be explained by the loss of a critical post-translational modification(s) in the recombinant protein, and/or different conditions experienced in lysate versus those experienced in buffer alone. Both EPHX2 and BCAT1 are known to be sensitive to the redox potential of their media[28,29], which may induce conformational changes affecting the binding and/or reactivity of the SAF. Compound **17** (not included in our library of 16 compounds), was found to react quantitatively and stoichiometrically with MIF after 16 h at 25 °C *in vitro*, as determined by LC-ESI-MS (Supplementary Fig. 3). Therefore, a standard curve comprised of serial dilutions from 3 μM to 37 nM in 3-fold decrements of recombinant MIF fully conjugated to

Author Manuscript Author Manuscript Author Manuscript Author Manuscript

17 and tetramethylrhodamine was included on each denaturing gel in order to quantify the extent of each reaction (Fig. 3a & Supplementary Fig. 4).

SAF-Reactive Sites on Three Target Proteins

To gain further insights into the SAF conjugation sites, we reacted three of the purified proteins with the SAF used to identify it from the human proteome in the presence of known active site inhibitors (Fig. 3). Conjugation was again confirmed by subjecting these *in vitro* reactions to a CuAAC reaction with TMR-N_3 and examining the results *via* SDS-PAGE. Addition of the validated MIF-reactive compound benzyl isothiocyanate (BITC; 50 μM), which forms a bond with the N-terminal proline residue (Pro1) of MIF[30] (Fig. 3c), to the reaction of recombinant MIF (5 μM) and **13** (50 μM) strongly attenuates conjugate formation (Fig. 3f). This suggests that SAF probe **13** reacts with Pro1 or a nearby residue. This result was further confirmed by LC-MS/MS analysis of the MIF•**13** conjugate (Supplementary Fig. 5). In similar fashion, addition of the documented EPHX2 non-covalent inhibitor TPPU[31] (Fig. 3d, 10 μM) to the reaction of recombinant EPHX2 (3 μM) with **9** (50 μM) largely ablates the fluorescence signal (Fig. 3g), indicating that **9** occupies the enzyme's active site. This site contains two tyrosine residues, Tyr383 and Tyr466, that carry out the hydrolysis of certain lipid epoxides[29]. Either of these two catalytic residues appeared to be a likely site of reaction between the SAFs and EPHX2, as both of them are susceptible to nitration[32]. Analysis of the EPHX2•**9** conjugate by LC-MS/MS implicates Tyr466 as the reactive residue in EPHX2 (Supplementary Fig. 6). It should be noted that **9** also contains an arylfluorosulfate; however, the reaction between **9** and EPHX2 occurs at the SAF electrophilic center, as this protein is enriched by other SAFs (**1** and **12**) which do not harbour arylfluorosulfates. To support the hypothesis that this reaction occurs at the SAF sulfur center and not the fluorosulfate, we subjected EPHX2 to reaction with an additional compound, **9***, that shares structural similarity with **9** but lacks a fluorosulfate. Subsequent analysis of the resulting conjugate by LC/MS-MS confirmed that the reaction between EPHX2 and **9*** takes place at Tyr466, the same residue that reacts with **9** (Supplementary Fig. 7). Carrying out a labeling reaction between PARP1cat and **2** in the presence of the PARP1 non-covalent inhibitor olaparib[33] (Fig. 3e) abolished covalent conjugate formation (Fig. 3h), indicating that **2** modifies PARP1 in the NAD^+ binding site[34]. By subjecting the reaction of **2** with PARP1cat to LC-MS/MS analysis, we determined that **2** reacts with Tyr907 in this site to form the PARP1•**2** conjugate (Supplementary Fig. 8). This was further confirmed by observing a strongly attenuated reaction between **2** and the Y907F mutant of PARP1cat (as compared to wild-type PARP1cat) (Supplementary Fig. 9). While we cannot completely rule out allosteric mechanisms of competition, the previously reported ligands BITC, TPPU, and olaparib appear to bind proximal to the SAF-reactive residues in MIF, EPHX2, and PARP1cat, respectively.

SAFs Inhibit PARP1 Activity *in Vitro*

PARP1 executes a critical signaling post-translation modification in response to single stranded DNA breaks. Using nicotinamide adenine dinucleotide (NAD^+), it mediates polymerization of ADP-ribose onto itself and other target proteins[35]. The newly synthesized poly(ADP-ribose) (PAR) chains act as a signal for recruitment of diverse families of proteins

Author Manuscript Author Manuscript Author Manuscript Author Manuscript

to the sites of DNA damage[36]. Given the status of PARP1 as a validated pharmacological target, we sought to confirm that the reaction with SAF probes inhibits the enzyme's activity. We examined the activity of PARP1 in the presence of selected SAFs, all sharing a common propargyl thymidine structure with the exception of **23** (Fig. 4a). Pre-incubation of PARP1 with activated damaged DNA and SAF compound for 20 min before addition of NAD^+ resulted in limited inhibition of PARP1, with the notable exception of **23** which exhibited substantial inhibition. However, significant inhibition was observed with **2** and **5** after an 18 h reaction period (Fig. 4b & 4c). Compound **23** shares considerable structural similarity with rucaparib, another FDA approved PARP1 inhibitor[37,38]. Examination of the co-crystal structure of PARP1cat bound to rucaparib (Fig. 4d, PDB: 4RV6)**,** led us to posit that the inhibitory effects of **23** are mediated primarily through non-covalent interactions with PARP1, in contrast to the considerable conjugation demonstrated by **2** and **5**. To test this hypothesis, we subjected **2**, **5**, **20**, and **23** to reactions with PARP1cat for 20 min or 18 h, followed by a CuAAC reaction with TMR-N_3. The results were quantified by fluorescent SDS-PAGE (Fig. 4e & 4f). It is clear that **23** did not react with PARP1cat above background. We hypothesize that **23** adopts a binding orientation close to that of rucaparib in the NAD^+-binding site of PARP1cat, preventing the SAF from engaging with Tyr907. On the other hand, SAFs **2** and **5** react substantially with PARP1cat, with some reaction occurring after just 20 min at 25 °C. These results suggest that simply modifying the existing structures of known protein ligands with SAF electrophiles does not result in a conjugation reaction, emphasizing the importance of proper positioning of the SAF.

SAF 2 Inhibits PAR Synthesis in HeLa Cells

To investigate whether SAFs inhibit PARP1 activity in living cells, we treated HeLa cells with either **2**, **5**, or olaparib for 24 h prior to addition of H_2O_2 for 15 min to induce PARylation. No immediate cell death was observed over this period. After cell lysis, the extent of PAR modification was measured by immunoblot using antibodies recognizing PAR and PARP1. Cells treated with **2** exhibited significant reduction in both general PARylation and PARP1 auto-modification, unlike cells treated with **5** or vehicle alone (Fig. 5a). As expected, treatment with olaparib (positive control) resulted in total ablation of PAR synthesis. The ability of **2** to inhibit PARP1 activity in cells is notable, given that its structure has not been optimized for cellular permeability nor PARP1 binding by medicinal chemistry efforts.

To scrutinize the cellular activity, we subjected HeLa cells to a 24 h treatment with either olaparib or **2**. Cells were then washed and fresh media (free of inhibitor) was added for 6 h. PARP1 activity was then induced via treatment with H_2O_2. This treatment regimen by **2** retained most of its PARP1 inhibitory activity, whereas olaparib activity was dramatically reduced (Fig. 5b), indicating that conjugation by **2** inhibits PAR synthesis until the enzyme is turned over.

Discussion

Past drug discovery efforts by and large have not deliberately leveraged functional groups capable of protein conjugation. This may be due to concerns about off-target reactivity and

Author Manuscript Author Manuscript Author Manuscript Author Manuscript

associated toxicity. However, the recent emergence of new functional groups that exhibit highly attenuated or latent protein reactivity, like those capable of undergoing a SuFEx reaction, suggest that drug discovery efforts making deliberate use of these functionalities could produce highly selective covalent drugs[2,6,26]. Our previous IDD approach with arylfluorosulfates led to validated covalent probes for eleven human proteins[4]. In this study, a new set of proteins closely associated with pathology (e.g., BCAT1, EPHX2, PARP1, and MIF) were matched with SAFs *via* the IDD strategy. Recombinant BCAT1 and EPHX2 exhibited low reactivity toward their corresponding SAF probes, suggesting that significant medicinal chemistry would be required to modulate function with SAFs. Conversely, MIF and PARP1 exhibited robust reactivity toward SAFs from our first-generation library, suggesting that discovery of more reactive and selective SAF compounds towards these proteins would likely require less effort. Notably, we demonstrated that **2** inhibited PARP1 function in living cancer cells even after compound washout, implying that SAF-based inhibition of PARP1 may represent a viable anticancer strategy.

Acquired or inherited defects in the DNA damage response and repair system increase the lifetime risk of cancer. Mutations in BRCA1 and BRCA2, both DNA repair proteins, were some of the first mutations to be associated with familial breast and ovarian cancers[39,40]. Targeting of PARP1 has been appealing since the 1980 demonstration that inhibition of PARP1 sensitized leukemia cells to cytotoxic alkylating agents[41]. This premise was built upon by an abundance of preclinical evidence supporting the ability of PARP inhibitors to sensitize and potentiate radiation and cytotoxic chemotherapy[42]. However, the pivotal breakthrough was made with the observation that BRCA-mutant (BRCAm) cells were up to 1000x more sensitive to PARP inhibitors[43,44]. The enhanced sensitivity observed in BRCAm cancer cells enabled the clinical validation of synthetic lethality in oncology, a concept first described in 1922, wherein simultaneous targeting of two genes or proteins can be lethal, even when deletion/inhibition of each individually is itself tolerated[45,46].

Treatment of cancers with existing PARP1 inhibitors is associated with a high incidence of toxicity (such as neutropenia and anemia)[47]. New PARP1 inhibitors based on a covalent mechanism of action may allow for circumvention of side effects associated with existing inhibitors. It has been recently reported that PAR synthesis helps drive α-synuclein aggregation both *in vitro* and *in vivo*, highlighting PARP1 inhibition as a potential therapy for the treatment of Parkinson's Disease[48]. Such a therapy would most likely require an extended duration of action, a convenient feature of SAF-based PARP1 inhibitors[49]. It is notable that our PARP1-reactive compounds bear little structural resemblance to the FDA-approved inhibitors (e.g., olaparib). These compounds represent a fresh start for inhibitor design and synthesis. Covalent PARP1 inhibitors may be optimized to achieve selective PARP1 or PARP2 inhibition, whereas non-covalent inhibitors are expected to bind to a wider array of PARP family members[38].

The apparent low reactivity of SAFs mean that only a subset of the human proteome is even capable of reacting with this functional group, significantly reducing off-target reactivity observed with more reactive electrophiles. This feature, combined with their chirality and straightforward synthesis, make SAFs ideally suited for the rapid generation of compound libraries, potentially simplifying medicinal chemistry-based optimization of identified hits.

Author Manuscript Author Manuscript Author Manuscript Author Manuscript

For IDD involving arylfluorosulfates, the electrophilic warhead and affinity handle must be installed at separate sites *via* separate reactions or judicious use of one-pot reaction schemes. As a result, the applicability of the arylfluorosulfates in library construction is more challenging. For these reasons, we recommend that future inverse drug discovery efforts take seriously the potential of SAFs.

Methods

Proteome labelling, fluorescence SDS-PAGE, and SAF-protein conjugate affinity purification

Conjugation reactions were carried out as follows: 5 μL of either DMSO or a 10 mM solution of SAF compound in DMSO was added to 995 μL of HEK293T lysate, followed by incubation at 25°C for 18 hours. Following the proteome reaction period, 50 μL of each reaction was subjected to copper(I)-catalyzed azide-alkyne cycloaddition (CuAAC) reaction conditions with tetramethylrhodamine-azide (TMR-N_3) (ThermoFisher Scientific). CuAAC conditions were as follows: 2 μL of 20 μM $CuSO_4$, 2 μL of 40 mM BTTAA (Click Chemistry Tools), 2.5 μL of sodium ascorbate (Sigma-Aldrich), and 1 μL of 5 mM TMR-N_3 (in DMSO) were added to 50 μL of each proteome labelling reaction, and reactions were incubated at 30 °C for 1 hour. Afterwards, proteins in the reaction mixture were precipitated by addition of MeOH/$CHCl_3$ (3:1). Proteins were resuspended and subsequently pelleted twice in MeOH to facilitate removal of excess TMR-N_3. Following final removal of MeOH by aspiration, proteins were dissolved in reducing sodium dodecyl sulfate (SDS) loading buffer. Proteins were resolved by SDS polyacrylamide gel electrophoresis (PAGE), and the fluorescently labelled proteins were visualized using a ChemiDoc XRS+ imager (Bio-Rad). Gels were then stained with a NOVEX® Colloidal Blue Stain Kit (Invitrogen) to assess equal protein loading across all lanes.

Protein-SAF conjugates were purified, digested, and TMT mass tagged in accordance with a published experimental procedure[4]. Briefly, 950 μL of each proteome conjugation reaction described in the immediately preceding section were subjected to CuAAC reaction conditions, substituting TMR-N_3 with diazo biotin azide (Biotin-N_3) (Click Chemistry Tools, catalog no. 1041). The reaction conditions were as follows: 20 μL of 20 μM $CuSO_4$, 20 μL of 40 mM BTTAA, 50 μL of sodium ascorbate, and 10 μL of 5 mM Biotin-$N_{3\ (DMSO)}$ were added to 950 μL of each proteome labelling reaction, and reactions were incubated at 30 °C for 2 hours. Following the CuAAC reaction, proteins subjected to the conjugation reaction were precipitated by addition of MeOH/$CHCl_3$ (3:1) and subsequently pelleted by centrifugation. The supernatant was removed by aspiration, and the pellet was washed with MeOH three times to remove excess biotin-N_3. After briefly drying pellets in air following removal of MeOH, proteome samples were resuspended in 6M urea solution containing 25 mM $(NH_4)HCO_3$. SDS (as a 10% solution w/v in water) was added to a final concentration of 2.2% to solubilize the protein pellets. Next, proteins were reduced by addition of 1M dithiothreitol (DTT) to a final concentration of 7.8 mM and incubation for 15 minutes at 65 °C. After cooling briefly on ice, the proteins were alkylated by addition of 0.5 M iodoacetamide (Sigma-Aldrich) to a final concentration of 29 mM and incubated in the dark for 30 minutes at 25°C. Proteome samples were each diluted into 6 mL of PBS containing

Author Manuscript Author Manuscript Author Manuscript Author Manuscript

High-Capacity Streptavidin Agarose Resin (ThermoFisher Scientific) and allowed to incubate for 16 hours with gentle agitation. The resin was then washed: once with PBS + 1% SDS, then twice with PBS containing no detergent. Labeled proteins were then eluted from the resin by incubating 1 hour at 25°C with PBS containing 1% SDS and 50 mM $Na_2S_2O_4$ (solution was quickly adjusted to pH ~7 following dissolution of $Na_2S_2O_4$). The elution procedure was carried out twice and the elution volumes combined. The subsequently enriched proteins were then precipitated once again with MeOH/$CHCl_3$ (3:1), the pellets were washed and centrifuged twice with MeOH to remove traces of SDS, and were then dried in air to remove residual MeOH. Proteins were then resuspended in a solution containing 0.2% Rapigest detergent (Waters) and 100 mM HEPES pH 8.0, and were digested overnight with mass-spectrometric grade trypsin protease (ThermoFisher Scientific). Digested samples were then reacted with their designated TMT 6-plex reagent (ThermoFisher Scientific) for 1 hour (reactions were conducted in 40% acetonitrile), the reactions were quenched by the addition of 10% $(NH_4)HCO_3$ (w/v) to a final concentration of 0.4% (w/v) for 1 hour. The quenched reactions were then combined and acidified to pH < 2 by the addition of formic acid. The acetonitrile used in the TMT-labeling reaction was removed via centrifugation under reduced pressure, and the samples were incubated at 42 °C for 1 hour to precipitate the remaining Rapigest. The samples were then centrifuged and the supernatants were collected and loaded into columns for multidimensional protein identification technology (MuDPIT) experiments, as previously described[50]. Heatmap was generated with R (version 3.2.4), using enrichment ratios for hand selected proteins identified by MuDPIT experiments.

Fluorescence-based analysis of reactions between select SAFs and select proteins

Reactions were carried out at room temperature in PBS (pH 7.4). Protein (MIF, BCAT1, EPHX2, or PARP1cat; 3 μM) were incubated with 30 μM of indicated SAF compound for 24 hours at room temperature. 50 μL of each reaction were subjected to CuAAC reaction conditions with TMR-N_3 (described previously). Reactions were then treated with 12 μL of 6x SDS loading buffer, followed by SDS-PAGE. The fluorescently labelled protein was visualized using a ChemiDoc XRS+ imager (Bio-Rad). Fluorescent bands were quantified using Image Lab (BioRad) and plotted using Prism 6 (GraphPad). Error bars represent ± standard error measurement for three independent experiments. Statistical significance was calculated with unpaired Student's t-test; ** $p \leq 0.01$, *** $p \leq 0.001$. The extent of SAF/protein reactions were quantified using fluorescent MIF standard curve. MIF (10 μM) in PBS was reacted with **17** (100 μM) for 24 hours at room temperature (≈25°C), after which time reaction completion was confirmed *via* liquid chromatography/mass spectrometric (LC-MS) analysis using a 1260 Infinity LC System (Agilent Technologies) and a 6130 Quadrupole LC/MS (Agilent Technologies). Protein *m/z* was calculated using the Deconvolution Tool in the OpenLab Software Sutie (Agilent Technologies). MIF was diluted to 3 μM in PBS and subject to CuAAC reaction conditions with TMR-N_3 (described previously). This solution was then diluted 3-fold five times into PBS containing SDS loading buffer to make the standard curve.

Author Manuscript Author Manuscript Author Manuscript Author Manuscript

Fluorescence-based analysis of the reaction between MIF and 13 (with or without BITC)

MIF (5 μM) in PBS was treated with **13** (50 μM) along with either 50 μM benzyl isothiocyanate (BITC) or an equivalent volume of DMSO. Reactions were carried out at room temperature for 24 hours. After such time, 50 μL of each reaction was subjected to CuAAC conditions with TMR-N_3 and subsequently treated with 12 μL of 6x SDS loading buffer, followed by SDS-PAGE. The fluorescently labelled protein was then visualized using a ChemiDoc XRS+ imager (Bio-Rad). Gels were then stained with a NOVEX® Colloidal Blue Stain Kit (Invitrogen) and imaged using a ChemiDoc XRS+ imager (Bio-Rad).

Fluorescence-based analysis of the reaction between EPHX2 and 9 (with or without TPPU)

EPHX2 (3 μM) in PBS was treated with **9** (50 μM) along with either 10 μM 1-trifluoromethoxyphenyl-3-(1-propionylpiperidin-4-yl) urea (TPPU) or an equivalent volume of DMSO. Reactions were carried out at room temperature for 24 hours. After such time, 50 μL of each reaction was subjected to CuAAC conditions with TMR-N_3 and subsequently treated with 12 μL of 6x SDS loading buffer, followed by SDS-PAGE. The fluorescently labelled protein was then visualized using a ChemiDoc XRS+ imager (Bio-Rad). Gels were then stained with a NOVEX® Colloidal Blue Stain Kit (Invitrogen) and imaged using a ChemiDoc XRS+ imager (Bio-Rad).

Fluorescence-based analysis of the reaction between PARP1cat and 2 (with or without olaparib)

PARP1cat (3 μM) in PBS was treated with **2** (100 μM) along with either 10 μM olaparib or an equivalent volume of DMSO. Reactions were carried out at room temperature for 24 hours. After such time, 50 μL of each reaction was subjected to CuAAC conditions with TMR-N_3 and subsequently treated with 12 μL of 6x SDS loading buffer, followed by SDS-PAGE. The fluorescently labelled protein was then visualized using a ChemiDoc XRS+ imager (Bio-Rad). Gels were then stained with a NOVEX® Colloidal Blue Stain Kit (Invitrogen) and imaged using a ChemiDoc XRS+ imager (Bio-Rad).

Data availability

Additional methods and data are provided in the Supplementary Information. All data generated or analyzed during this study are included in this published article (and its supplementary files).

Supplementary Material

Refer to Web version on PubMed Central for supplementary material.

Acknowledgements

This work was supported by the Skaggs Institute for Chemical Biology, the Lita Annenberg Hazen Foundation, and by National Institutes of Health grants DK046335 (J.W.K.). R.C.B. was supported by a grant from the American Cancer Society. D.E.M. was supported by a grant from the George E. Hewitt Foundation for Medical Research. This work was supported in part by the National Institute of Environmental Health Sciences (NIEHS) Grant R01 ES002710, and NIEHS Superfund Research Program P42 ES004699.

Author Manuscript Author Manuscript Author Manuscript Author Manuscript

References

1. Macarron R et al. Impact of high-throughput screening in biomedical research. Nat Rev. Drug Disc. 10, 188–195 (2011).
2. Singh J, Petter RC, Baillie TA & Whitty A The resurgence of covalent drugs. Nat Rev. Drug Disc 10, 307 (2011).
3. Bauer RA Covalent inhibitors in drug discovery: from accidental discoveries to avoided liabilities and designed therapies. Drug Discovery Today 20, 1061–1073 (2015). [PubMed: 26002380]
4. Mortenson DE et al. “Inverse Drug Discovery” Strategy To Identify Proteins That Are Targeted by Latent Electrophiles As Exemplified by Aryl Fluorosulfates. J. Am. Chem. Soc 140, 200–210 (2018). [PubMed: 29265822]
5. Dong J, Krasnova L, Finn MG & Sharpless KB Sulfur(VI) Fluoride Exchange (SuFEx): Another Good Reaction for Click Chemistry. Angew. Chem. Int. Ed. Engl 53, 9430–9448 (2014). [PubMed: 25112519]
6. Chen W et al. Arylfluorosulfates Inactivate Intracellular Lipid Binding Protein(s) through Chemoselective SuFEx Reaction with a Binding Site Tyr Residue. J. Am. Chem. Soc 138, 7353–7364 (2016). [PubMed: 27191344]
7. Dong J, Sharpless KB, Kwisnek L, Oakdale JS & Fokin VV SuFEx-Based Synthesis of Polysulfates. Angew. Chem. Int. Ed. Engl 53, 9466–9470 (2014). [PubMed: 25100330]
8. Gao B et al. Bifluoride-catalysed sulfur(VI) fluoride exchange reaction for the synthesis of polysulfates and polysulfonates. Nat Chem. 9, 1083 (2017). [PubMed: 29064495]
9. Wang H et al. SuFEx-Based Polysulfonate Formation from Ethenesulfonyl Fluoride–Amine Adducts. Angew. Chem. Int. Ed. Engl 56, 11203–11208 (2017). [PubMed: 28792119]
10. Liu Z et al. SuFEx Click Chemistry Enabled Late-Stage Drug Functionalization. J. Am. Chem. Soc 140, 2919–2925 (2018). [PubMed: 29451783]
11. Li S, Wu P, Moses JE & Sharpless KB Multidimensional SuFEx Click Chemistry: Sequential Sulfur(VI) Fluoride Exchange Connections of Diverse Modules Launched From An SOF4 Hub. Angew. Chem. Int. Ed. Engl 56, 2903–2908 (2017). [PubMed: 28165188]
12. Wang Q et al. Bioconjugation by Copper(I)-Catalyzed Azide-Alkyne [3 + 2] Cycloaddition. J. Am. Chem. Soc 125, 3192–3193 (2003). [PubMed: 12630856]
13. Rostovtsev VV, Green LG, Fokin VV & Sharpless KB A Stepwise Huisgen Cycloaddition Process: Copper(I)-Catalyzed Regioselective “Ligation” of Azides and Terminal Alkynes. Angew. Chem. Int. Ed. Engl 41, 2596–2599 (2002). [PubMed: 12203546]
14. Verhelst SH, Fonovic M & Bogyo M A mild chemically cleavable linker system for functional proteomic applications. Angew. Chem. Int. Ed. Engl 46, 1284–1286 (2007). [PubMed: 17205587]
15. Dayon L et al. Relative Quantification of Proteins in Human Cerebrospinal Fluids by MS/MS Using 6-Plex Isobaric Tags. Anal Chem. 80, 2921–2931 (2008). [PubMed: 18312001]
16. Konecny GE & Kristeleit RS PARP inhibitors for BRCA1/2-mutated and sporadic ovarian cancer: current practice and future directions. Br J. Cancer 115, 1157 (2016). [PubMed: 27736844]
17. Lord CJ & Ashworth A BRCAness revisited. Nat Rev. Cancer 16, 110 (2016). [PubMed: 26775620]
18. Lue H, Kleemann R, Calandra T, Roger T & Bernhagen J Macrophage migration inhibitory factor (MIF): mechanisms of action and role in disease. Microbes and Infection 4, 449–460 (2002). [PubMed: 11932196]
19. Calandra T & Roger T Macrophage migration inhibitory factor: a regulator of innate immunity. Nat Rev. Immunol. 3, 791 (2003). [PubMed: 14502271]
20. Imig JD & Hammock BD Soluble epoxide hydrolase as a therapeutic target for cardiovascular diseases. Nat. Rev. Drug Disc. 8, 794 (2009).
21. Tonjes M et al. BCAT1 promotes cell proliferation through amino acid catabolism in gliomas carrying wild-type IDH1. Nat Med. 19, 901–908 (2013). [PubMed: 23793099]
22. Xu M et al. BCAT1 promotes tumor cell migration and invasion in hepatocellular carcinoma. Oncology letters 12, 2648–2656 (2016). [PubMed: 27698837]

Author Manuscript Author Manuscript Author Manuscript Author Manuscript

23. Zhang L & Han J Branched-chain amino acid transaminase 1 (BCAT1) promotes the growth of breast cancer cells through improving mTOR-mediated mitochondrial biogenesis and function. Biochem Biophys. Res. Commun 486, 224–231 (2017). [PubMed: 28235484]
24. Zhao Q et al. Broad-Spectrum Kinase Profiling in Live Cells with Lysine-Targeted Sulfonyl Fluoride Probes. J. Am. Chem. Soc 139, 680–685 (2017). [PubMed: 28051857]
25. Zheng Q et al. SuFEx-enabled, agnostic discovery of covalent inhibitors of human neutrophil elastase. Proc. Natl. Acad. Sci. U S A 116, 18808–18814 (2019). [PubMed: 31484779]
26. Hett EC et al. Rational Targeting of Active-Site Tyrosine Residues Using Sulfonyl Fluoride Probes. ACS Chem Biol. 10, 1094–1098 (2015). [PubMed: 25571984]
27. Hanoulle X et al. A new functional, chemical proteomics technology to identify purine nucleotide binding sites in complex proteomes. J. Proteome Res 5, 3438–3445 (2006). [PubMed: 17137346]
28. Goto M et al. Structural Determinants for Branched-chain Aminotransferase Isozyme-specific Inhibition by the Anticonvulsant Drug Gabapentin. J Biol. Chem 280, 37246–37256 (2005). [PubMed: 16141215]
29. Morisseau C & Hammock BD Epoxide Hydrolases: Mechanisms, Inhibitor Designs, and Biological Roles. Ann Rev. Pharmacol. Toxicol 45, 311–333 (2005). [PubMed: 15822179]
30. Spencer ES et al. Multiple binding modes of isothiocyanates that inhibit macrophage migration inhibitory factor. Eur J. Med. Chem 93, 501–510 (2015). [PubMed: 25743213]
31. Lee KS et al. Optimized inhibitors of soluble epoxide hydrolase improve in vitro target residence time and in vivo efficacy. J Med. Chem 57, 7016–7030 (2014). [PubMed: 25079952]
32. Barbosa-Sicard E et al. Inhibition of the soluble epoxide hydrolase by tyrosine nitration. J Biol. Chem 284, 28156–28163 (2009). [PubMed: 19704161]
33. Fong PC et al. Inhibition of poly(ADP-ribose) polymerase in tumors from BRCA mutation carriers. N Engl. J. Med 361, 123–134 (2009). [PubMed: 19553641]
34. Dawicki-McKenna, Jennine M. et al. PARP-1 Activation Requires Local Unfolding of an Autoinhibitory Domain. Molecular Cell 60, 755–768 (2015). [PubMed: 26626480]
35. Langelier M-F, Servent KM, Rogers EE & Pascal JM A Third Zinc-binding Domain of Human Poly(ADP-ribose) Polymerase-1 Coordinates DNA-dependent Enzyme Activation. J Biol. Chem 283, 4105–4114 (2008). [PubMed: 18055453]
36. Gibson BA & Kraus WL New insights into the molecular and cellular functions of poly(ADP-ribose) and PARPs. Nat Rev. Mol. Cell Biol 13, 411 (2012). [PubMed: 22713970]
37. Coleman RL et al. Rucaparib maintenance treatment for recurrent ovarian carcinoma after response to platinum therapy (ARIEL3): a randomised, double-blind, placebo-controlled, phase 3 trial. The Lancet 390, 1949–1961 (2017).
38. Thorsell A-G et al. Structural Basis for Potency and Promiscuity in Poly(ADP-ribose) Polymerase (PARP) and Tankyrase Inhibitors. J Med. Chem 60, 1262–1271 (2017). [PubMed: 28001384]
39. Futreal P et al. BRCA1 mutations in primary breast and ovarian carcinomas. Science 266, 120–122 (1994). [PubMed: 7939630]
40. Wooster R et al. Identification of the breast cancer susceptibility gene BRCA2. Nature 378, 789 (1995). [PubMed: 8524414]
41. Durkacz BW, Omidiji O, Gray DA & Shall S (ADP-ribose)n participates in DNA excision repair. Nature 283, 593 (1980). [PubMed: 6243744]
42. Tentori L & Graziani G Chemopotentiation by PARP inhibitors in cancer therapy. Pharmacol Res. 52, 25–33 (2005). [PubMed: 15911331]
43. Bryant HE et al. Specific killing of BRCA2-deficient tumours with inhibitors of poly(ADP-ribose) polymerase. Nature 434, 913 (2005). [PubMed: 15829966]
44. Farmer H et al. Targeting the DNA repair defect in BRCA mutant cells as a therapeutic strategy. Nature 434, 917 (2005). [PubMed: 15829967]
45. Nijman SMB Synthetic lethality: General principles, utility and detection using genetic screens in human cells. FEBS Lett. 585, 1–6 (2011). [PubMed: 21094158]
46. Bridges CB The Origin of Variations in Sexual and Sex-Limited Characters. The American Naturalist 56, 51–63 (1922).

Author Manuscript Author Manuscript Author Manuscript Author Manuscript

47. Pujade-Lauraine E et al. Olaparib tablets as maintenance therapy in patients with platinum-sensitive, relapsed ovarian cancer and a BRCA1/2 mutation (SOLO2/ENGOT-Ov21): a double-blind, randomised, placebo-controlled, phase 3 trial. The Lancet Oncology 18, 1274–1284 (2017). [PubMed: 28754483]

48. Kam T-I et al. Poly(ADP-ribose) drives pathologic α-synuclein neurodegeneration in Parkinson's disease. Science 362, eaat8407 (2018). [PubMed: 30385548]

49. Berger NA et al. Opportunities for the repurposing of PARP inhibitors for the therapy of non-oncological diseases. Br J. Pharmacol 175, 192–222 (2018). [PubMed: 28213892]

50. Ryno LM et al. Characterizing the altered cellular proteome induced by the stress-independent activation of heat shock factor 1. ACS Chem Biol 9, 1273–1283 (2014). [PubMed: 24689980]

Author Manuscript Author Manuscript Author Manuscript Author Manuscript

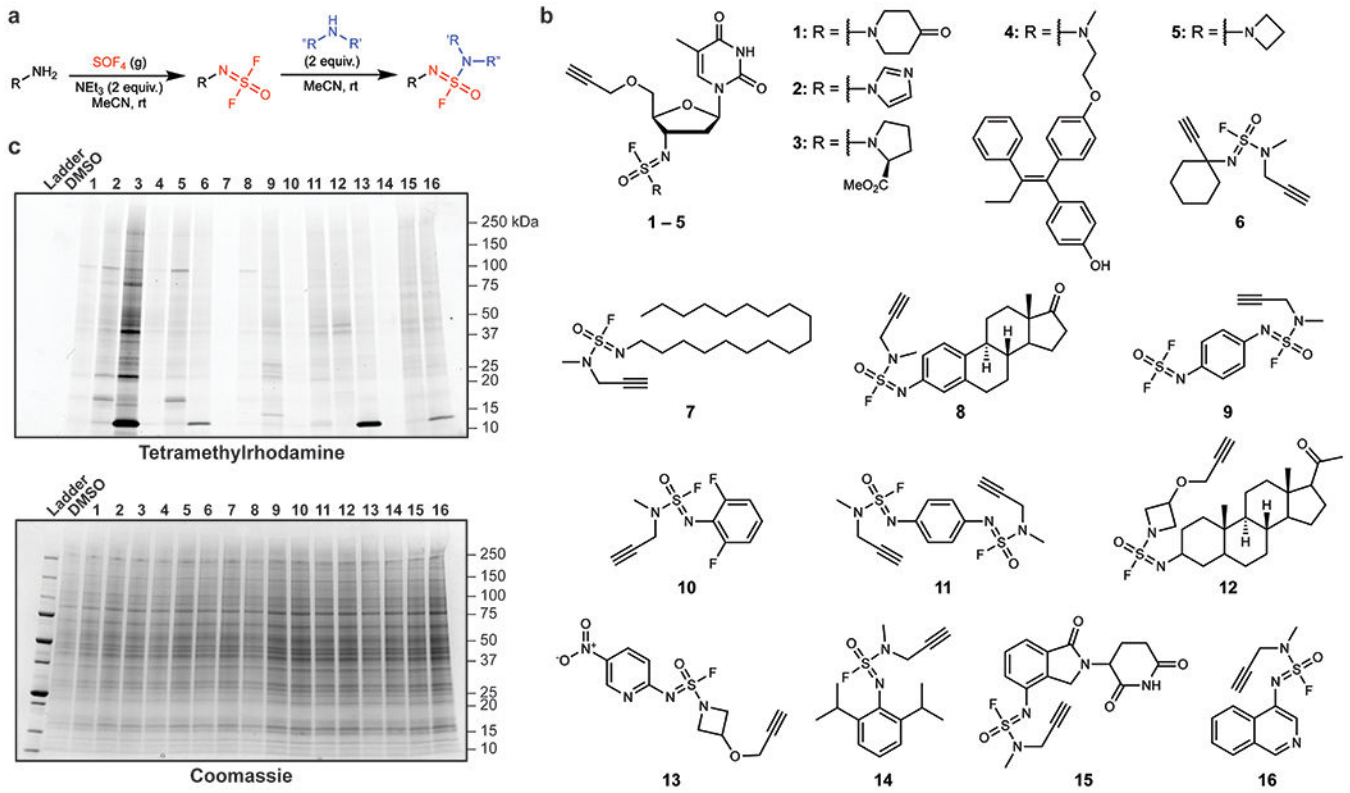

Fig. 1:

SAFs **1**–**16** react with proteins in HEK293T cell lysate. **a**) Stepwise synthetic scheme for the synthesis of SAF-containing compounds. A primary amine is reacted with SOF_4 to form an iminosulfur oxydifluoride (in red). This intermediate is then reacted with a secondary amine (in blue) to form an SAF. **b**) Structures of SAF Compounds **1**–**16** used in this study. **c**) *Top*: SDS-PAGE/rhodamine analysis of HEK293T lysate incubated (18 h) with SAF compound (50 μM), after addition of TMR-N_3 via CuAAC (see Experimental Section for detailed conditions). Each SAF appears to react with a different set of proteins, as indicated by the different banding patterns in each lane. *Bottom*: Coomassie stain of SDS-PAGE gel indicates equal loading of protein in each lane. Fluorescence intensity of each band is a product of SAF reactivity towards that protein rather than a difference in protein abundance between treated HEK293T lysates. This experiment was conducted twice (n=2) with similar results.

Author Manuscript Author Manuscript Author Manuscript Author Manuscript

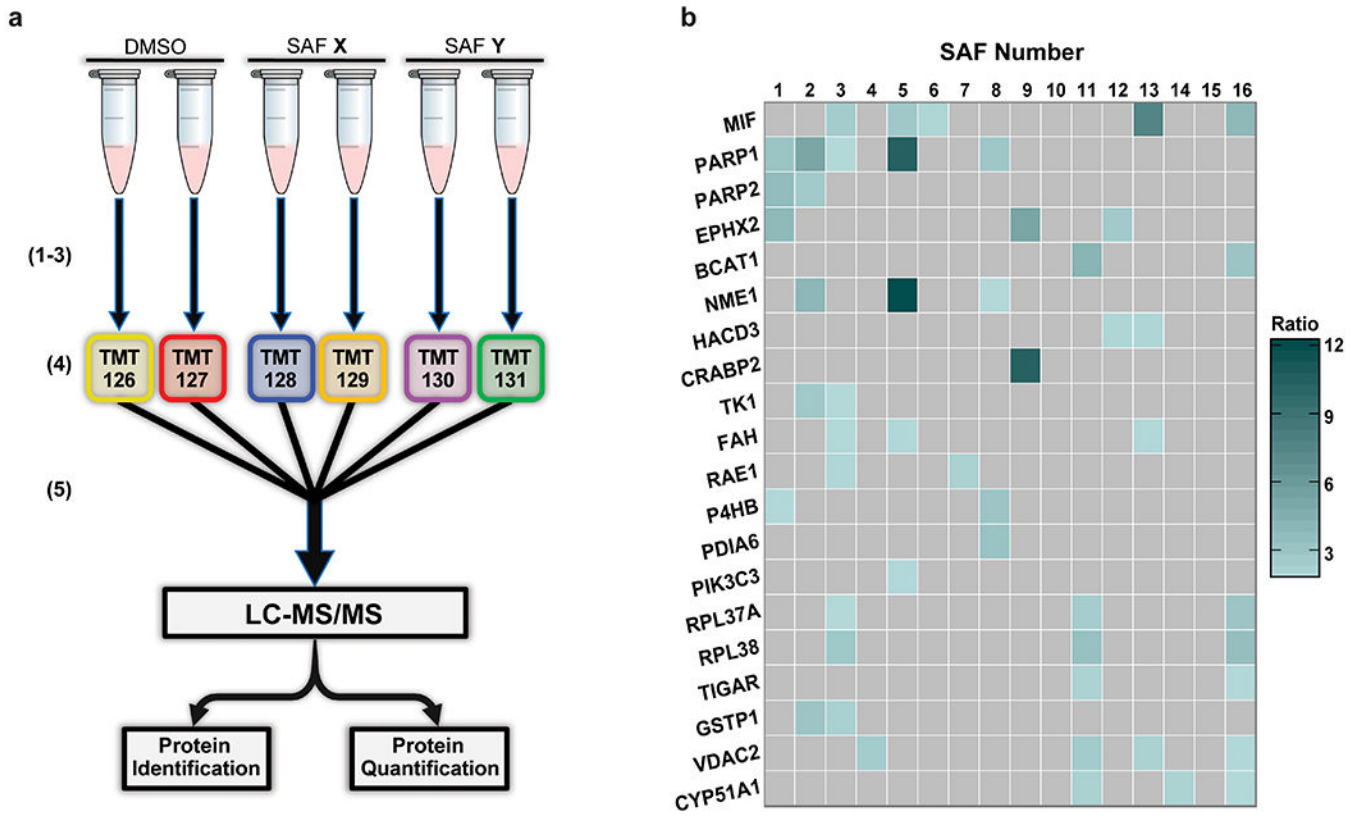

Fig. 2:

Proteins targeted by SAFs **1**–**16** identified using isobaric tandem mass tagging in conjunction with proteomic mass spectrometry. **a)** Tandem Mass Tagging LC-MS/MS workflow. After HEK293T lysate is treated with a particular probe (50 μM) for 18 h, they are **(1)** subject to CuAAC with Biotin-N_3. Next, **(2)** the protein-probe conjugates are enriched using Streptavidin resin, and the bound proteins are eluted from the resin using $Na_2S_2O_4$. The enriched conjugates are then **(3)** digested with trypsin, and the resulting peptides **(4)** are labeled with the respective TMT reagent. The tagged peptides **(5)** are pooled and subject to Multi-Dimensional Protein Identification Technology (MuDPIT) based LC-MS/MS, which allows for protein identification and quantification compared to DMSO controls. **b)** Heat map displaying enrichment ratios of probes **1**–**16** for select proteins by quantitative LC-MS/MS. Displayed proteins have enrichment ratios > 1.50 (treated samples vs. DMSO control), and p-values < 0.25 (calculated by two-tailed, unpaired t-test). Grey square indicates failure to make this cutoff. Data are the result of a single experiment containing two replicate treatment conditions (n=2). See Supplementary information for precise enrichment ratios and exact p-values.

Author Manuscript
Author Manuscript
Author Manuscript
Author Manuscript

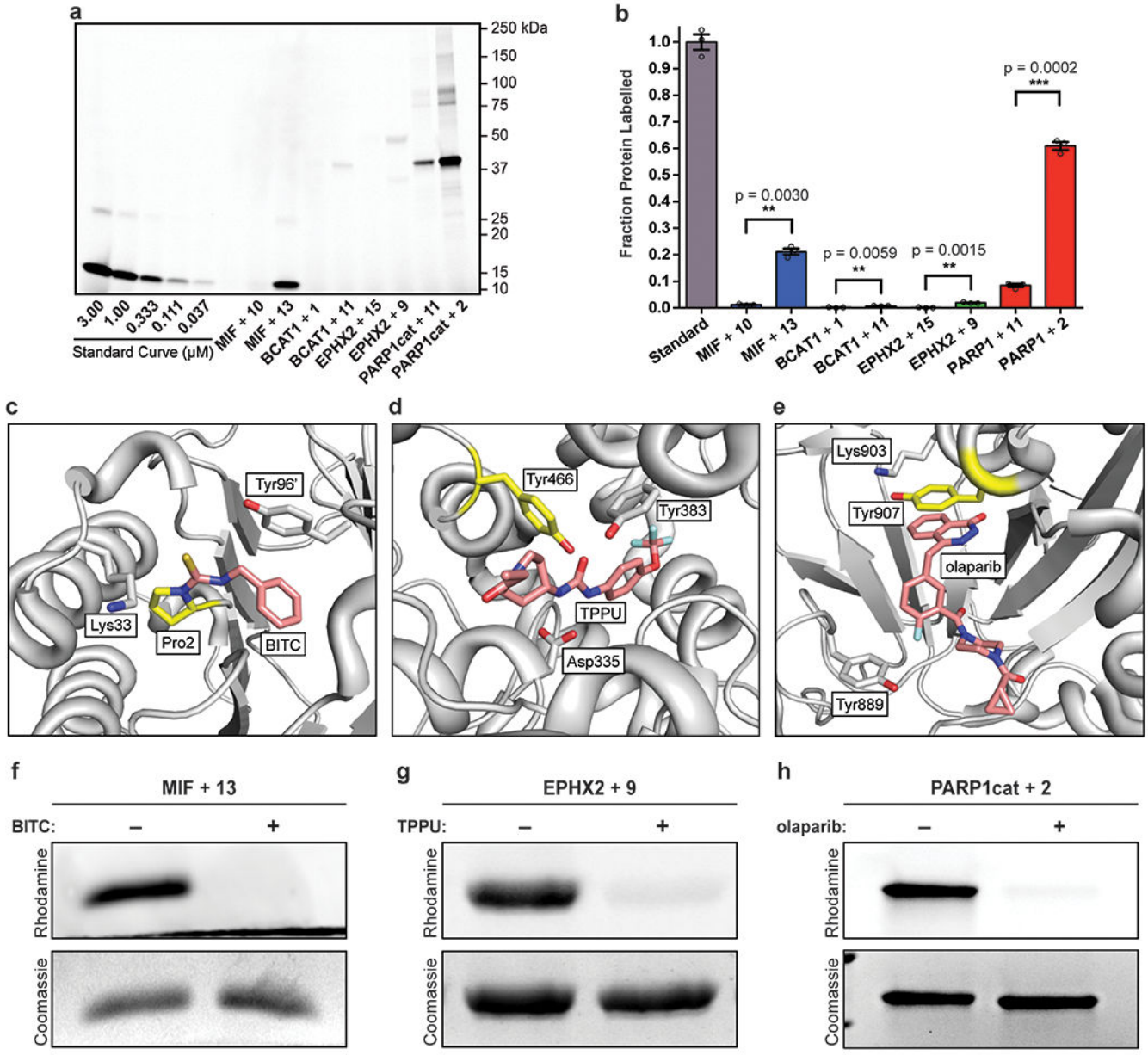

Fig. 3:

Validation of reactions between SAFs and select recombinant proteins. **a**) Fluorescence-based analysis of reactions (24 h) between select SAFs (30 μM) and select proteins (3 μM). Standard curve is comprised of four 3-fold dilutions of fluorescently labelled MIF (3.00 to 0.037 μM). This gel is representative of three independent experiments (n=3). **b**) Quantification of fluorescence bands in **a**. Error bars represent ± SEM for 3 independent experiments (n=3). P-values were calculated using a two-tailed, unpaired t-test, with ** $p \leq 0.01$, *** $p \leq 0.001$, exact P values displayed within figure panel. **c**) X-ray crystal structure of MIF conjugated to BITC, with Tyr95' from the adjacent monomer (PDB: 3WNT). **d**) X-ray crystal structure of EPHX2 bound to TPPU (PDB: 4OD0). **e**) X-ray crystal structure of PARP1 catalytic domain bound to olaparib (PDB: 5DS3). Residues highlighted in yellow

Author Manuscript Author Manuscript Author Manuscript Author Manuscript

denote the SAF-reactive nucleophiles identified by LC-MS/MS. Other labelled residues denote other potential binding site nucleophiles indicate and/or residues that may important for reaction with the SAFs (**c**, **d**, & **e**). **f**) Fluorescence-based analysis of the reaction of MIF (5 μM) and **13** (50 μM) for 24 h in the presence or absence of benzyl isothiocyanate (BITC; 50 μM). This experiment was conducted a single time (n=1). **g**) Fluorescence-based analysis of the reaction of EPHX2 (3 μM) and **9** (50 μM) for 24 h in the presence or absence of TPPU (10 μM). This experiment was conducted a single time (n=1). **h**) Fluorescence-based analyses of the reaction of PARP1cat (3 μM) with **2** (100 μM) for 24 h in the presence or absence of olaparib (10 μM). This experiment was conducted a single time (n=1).

Author Manuscript Author Manuscript Author Manuscript Author Manuscript

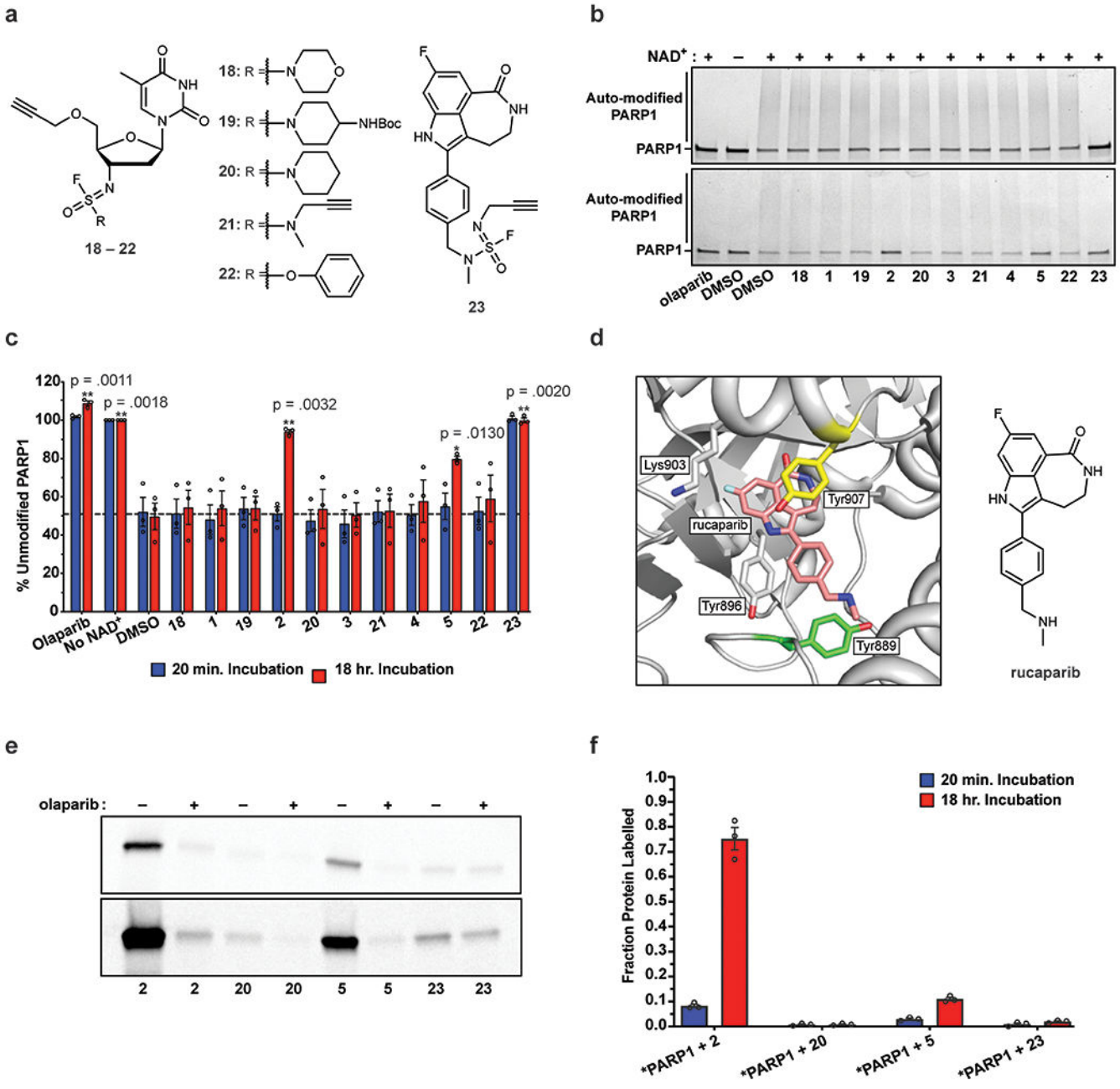

Fig. 4:

Analysis of PARP1 inhibitory activity of a subset of SAFs. **a**) Structures of SAFs **18** – **23** used in PARP1 auto-modification assay. *Left:* the structures of **18** – **22**, which all share a common thymidine core structure, with the affixed 2° amine differing between them. *Right:* Structure of compound **23**. None of these compounds were subjected to the IDD workflow (see Fig. 2a) used to identify SAF-reactive proteins. **b**) SDS-PAGE analysis of *in vitro* assay of PARP1 activity. PARP1 was incubated with the indicated compound for either 20 minutes (*top*) or 18 hours (*bottom*), then NAD^+ (100 μM) was added. Auto-modification reactions were run for 1 hour at room temperature before analysis. **c**) Quantification of SDS-PAGE in

Author Manuscript Author Manuscript Author Manuscript Author Manuscript

b. Error bars represent ± SEM for three independent experiments (n=3). P-values were determined using a two-tailed, paired t-test, with * p-value ≤ 0.05, ** p-value ≤ 0.01, and "n.s." p-value > 0.05 compared to samples treated with DMSO (See Source Data for analysis and exact p-values). Dashed line at 53.5% indicates approximate baseline of unmodified PARP1 *in vitro* (average between vehicle treatments at 20 minutes and 18 hours). **d**) *Left*: X-ray crystal structure of rucaparib bound in the NAD^+ binding site of PARP1cat (PDB: 4RV6). Tyr907 (the SAF-reactive residue) is highlighted in yellow, while proximal Tyr889 is highlighted green. Rucaparib is highlighted in pink. *Right*: The structure of FDA-approved PARP1 inhibitor rucaparib. **e**) In-Gel fluorescence analysis of reactions between PARP1cat (3 μM) and select SAF probes (30 μM). Olaparib (30 μM) was added as a control to negate reaction within the NAD^+ binding site of PARP1cat. PARP1cat was incubated with the indicated compound for either 20 minutes (*top*) or 18 hours (*bottom*) before subjecting reactions to CuAAC conditions. **f**) Quantification of in-gel fluorescence in **e**. Error bars represent ± SEM for three independent experiments (n=3). Results from reactions containing olaparib were omitted for clarity.

Author Manuscript Author Manuscript Author Manuscript Author Manuscript

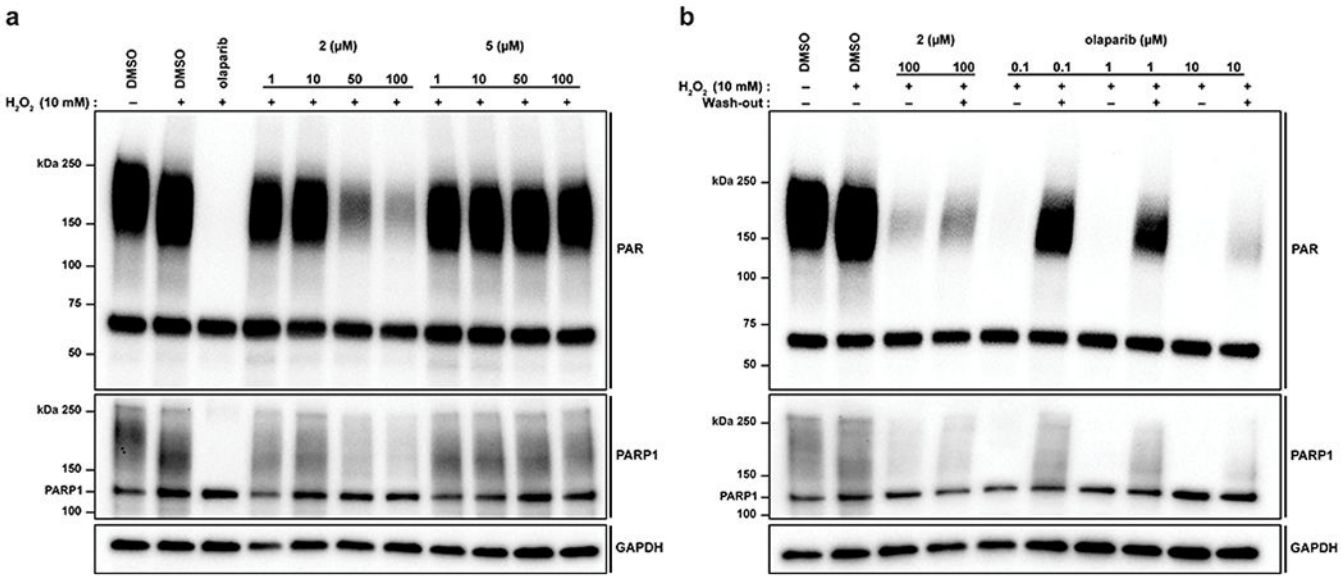

Fig. 5:

SAF **2** irreversibly inhibits the activity of PARP1 in HeLa cells. **a**) Western blot analysis of PARylation in HeLa cells treated with SAFs. Cells were incubated with either olaparib (ola; positive control), **2,** or **5** at increasing concentrations for 24 hours before addition of H_2O_2 (10 mM). Blots were analyzed with antibodies targeting either PAR (*top*) and PARP1 (*middle*). The reduction of both PAR and PAR-modified PARP1 (i.e., higher molecular weight smear in middle panel) indicates inhibition of PARP1's enzymatic activity. This experiment was conducted a single time (n=1). **b**) Western blot analysis of PARylation after HeLa cells were treated with either **2** (100 μM) or olaparib (0.1–10 μM) for 24 hours, and compounds were removed by washing cells twice with with PBS (pH 7.4). Blots were analyzed with antibodies targeting either PAR (*top*) and PARP1 (*middle*). The reduction of both PAR and PAR-modified PARP1 in cells treated with **2** and washed indicate that **2** is inhibiting PARP1 irreversibly. This experiment was conducted a single time (n=1).